IET Communications

WILEY

The Institution of Engineering and Technology

ORIGINAL RESEARCH OPEN ACCESS

Channel Estimation for Indoor Terahertz UM-MIMO: A Deep Learning Perspective for 6G Applications

Sakhshra Monga[1] | Gunjan Garg[1] | Nitin Saluja[1] | Olutayo Oyeyemi Oyerinde[2]

[1]Chitkara University Institute of Engineering and Technology, Chitkara University, Rajpura, Punjab, India | [2]School of Electrical and Information Engineering, University of the Witwatersrand, Johannesburg, South Africa

Correspondence: Sakhshra Monga (sakhshra@chitkara.edu.in)

Received: 1 April 2025 | **Revised:** 7 May 2025 | **Accepted:** 25 May 2025

Funding: The authors received no specific funding for this work.

ABSTRACT

The emergence of terahertz (THz) communication in ultra-massive multiple-input multiple-output (UM-MIMO) systems presents new challenges for accurate and efficient channel estimation, particularly under hybrid-field propagation conditions. Conventional estimation techniques struggle to meet the demands of such high-dimensional systems, especially in the presence of limited radio frequency (RF) chains and mixed near- and far-field effects. To address these limitations, this paper proposes a deep learning-based framework that combines a fully connected neural network (FCNN) for linear channel estimation with a convolutional neural network (CNN) for non-linear refinement. The architecture is designed to adapt to diverse propagation environments while maintaining computational efficiency. Simulation studies based on realistic THz scenarios demonstrate that the proposed approach significantly improves estimation accuracy, achieving up to 90% reduction in normalized mean squared error (NMSE) compared to traditional and advanced estimation techniques. The robustness of the model under varying signal-to-noise ratios and noise power levels underscores its potential for deployment in future 6G THz communication networks.

1 | Introduction

The terahertz (THz) band, spanning 0.1 to 10 THz, promises vast bandwidth for sixth-generation (6G) wireless networks, meeting the growing demand for high-speed data [1, 2]. Its short wavelengths enable ultra-massive multiple-input multiple-output (UM-MIMO) systems, packing thousands of antennas into compact arrays for precise, directional transmissions via advanced beamforming [3]. Yet, harnessing THz potential requires overcoming signal dispersion and molecular absorption, which degrade coverage [3], and demands accurate channel estimation with minimal pilot overhead in high-dimensional settings [4, 5]. Recent comprehensive surveys have identified data scarcity as a critical challenge impacting the training of deep learning models, particularly in scenarios where obtaining large labeled datasets is impractical. To address this limitation, techniques such as transfer learning, self-supervised learning, and GAN-based data augmentation have been widely explored to improve model robustness under constrained data environments [6, 7]. Additionally, specialized strategies like DeepSMOTE and physics-informed neural networks (PINNs) have been proposed to further alleviate data insufficiency issues across various fields, including wireless communications, healthcare, and structural health monitoring.

The planar array-of-subarray (AoSA) architecture, shown in Figure 1, offers a practical solution for THz UM-MIMO [8]. Antenna elements (AEs) form planar subarrays (SAs), each tied to a single radio frequency (RF) chain through phase shifters [9]. This setup reduces hardware costs and power use, with closely spaced AEs boosting array gain and widely spaced SAs preserving spatial multiplexing [10]. However, challenges arise:

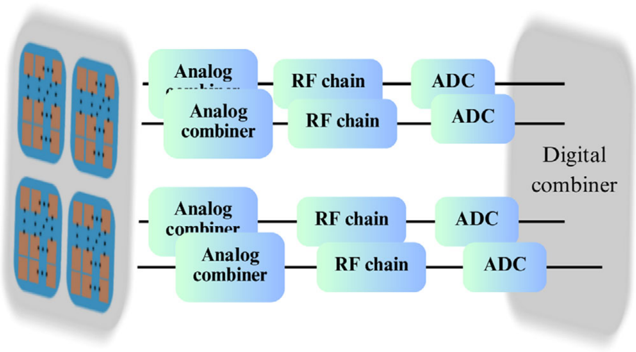

FIGURE 1 | Hybrid analog-digital channel estimation framework.

limited RF chains compress pilot signals, creating an underdetermined estimation problem [11]. The non-uniform array, unlike uniform designs in prior work, complicates universal algorithms, while the large aperture and short wavelengths introduce near-field effects alongside far-field paths, forming hybrid-field channels [12]. Traditional methods, built for uniform arrays in either far-field or near-field alone, falter under these real-world conditions [13].

This paper proposes a deep learning framework to address these issues, merging a fully connected neural network (FCNN) for linear estimation and a convolutional neural network (CNN) for non-linear refinement within a fixed point network (FPN) structure. Tailored to the hybrid-field THz UM-MIMO channel, it achieves precise estimation with low overhead, outperforming conventional and advanced techniques. The following sections detail the system model, methodology, and results, advancing efficient channel estimation for 6G networks. Table 1 shows abbreviations.

1.1 | Related Works

Channel estimation in terahertz (THz) ultra-massive multiple-input multiple-output (UM-MIMO) systems presents a fundamental challenge due to the limited availability of radio frequency (RF) chains, which imposes a significant pilot overhead when employing traditional least squares (LS) methods. These conventional approaches require pilot signals that scale with the channel dimension to achieve acceptable estimation accuracy. To mitigate this burden, compressed sensing (CS) and related techniques have been explored, leveraging *channel priors* to reduce the required pilot overhead. Broadly, existing strategies can be categorized into three methodological classes—sparse reconstruction, Bayesian inference, and deep learning (DL)—each offering unique advantages and limitations, as summarized in Table 2.

Sparse reconstruction hinges on crafting a dictionary matrix to cast the channel as a sparse vector, turning estimation into a recovery problem solvable with CS algorithms. For uniform arrays in the far field, a discrete Fourier transform (DFT) dictionary works well, reflecting angular sparsity. But in the near field, angle and distance both matter, demanding custom grids that prior far-field dictionaries can't handle [14]. Hybrid-field setups, like those in THz AoSA arrays, muddy the waters further—

TABLE 1 | Complete list of acronyms used in the paper.

Acronym	Description
CNN	Convolutional neural network
FCNN	Fully connected neural network
LS	Least squares
OMP	Orthogonal matching pursuit
OAMP	Orthogonal approximate message passing
FISTA	Fast iterative shrinkage-thresholding algorithm
EM-GEC	Expectation maximization-generalized expectation consistent
ISTA-Net	Iterative shrinkage-thresholding algorithm network
FPN-OAMP	Fixed point network for OAMP
NMSE	Normalized mean squared error
THz	Terahertz
UM-MIMO	Ultra-massive multiple-input multiple-output
IRS	Intelligent reflecting surface
SNR	Signal-to-noise ratio
SGD	Stochastic gradient descent
MSE	Mean squared error
LoS	Line-of-sight
NLoS	Non-line-of-sight
6G	Sixth-generation wireless network
MIMO	Multiple-input multiple-output
AI	Artificial intelligence
RL	Reinforcement learning
DNN	Deep neural network
MAB	Multi-armed bandit
HRL	Hierarchical reinforcement learning
DQN	Deep Q-network
BS	Base station
IoT	Internet of things

dictionary learning from site-specific data is the go-to fix, yet it struggles to adapt across locations [15].

Bayesian methods leverage prior knowledge of the channel distribution to enhance estimation accuracy, often employing iterative algorithms such as approximate message passing (AMP) for efficient inference when such *channel priori* are available [16]. However, in practical scenarios, true priors are typically unknown or difficult to model precisely. To address this, researchers adopt empirical approximations—such as Gaussian mixture models or hidden Markov chains—optimized through expectation-maximization (EM) techniques [17]. While structured priors yield high accuracy when well-aligned with the actual channel characteristics, their performance degrades significantly under model mismatch, which is common in hybrid-field THz environments.

TABLE 2 | Summary of channel estimation approaches for THz UM-MIMO.

Category	Key techniques	Strengths and Limitations
Sparse reconstruction	Dictionary matrices (DFT-based for far-field, custom grids for near-field), CS recovery [14, 15]	Works well for uniform far-field arrays; struggles with near-field and hybrid-field generalization.
Bayesian methods	AMP, EM-driven prior tuning, structured/unstructured priors [16, 17]	High accuracy with known priors; less effective in complex, unknown THz conditions.
Deep learning	Data-driven mapping, deep unfolding of iterative solvers [18, 19]	Handles complexity well; limited by scalability, adaptability, and out-of-distribution performance.

In contrast, unstructured priors offer greater adaptability at the cost of reduced precision, highlighting a trade-off between generalizability and estimation accuracy.

Deep learning approaches circumvent the need for explicit priors by learning intrinsic channel characteristics directly from data. In purely data-driven frameworks, pilot signals are mapped to channel estimates through end-to-end neural architectures, offering fast inference but often lacking interpretability and an understanding of the underlying measurement process [18]. To address this, model-driven techniques—commonly referred to as deep unfolding—transform traditional iterative solvers into structured neural networks with trainable parameters [19]. This hybrid design preserves algorithmic transparency while enhancing estimation accuracy. However, deep unfolding methods encounter several practical challenges: scaling to large antenna arrays significantly increases memory requirements, fixed-layer architectures restrict adaptability, and convergence is not always assured. Moreover, their performance tends to degrade when applied to scenarios that deviate from the training distribution—a frequent occurrence in dynamic THz environments characterized by hybrid propagation paths and intermittent blockages. These limitations underscore the need for more robust and adaptive channel estimation frameworks, motivating the approach proposed in this work for THz UM-MIMO systems.

1.2 | Contributions

This paper proposes a deep learning framework, termed fixed point networks (FPNs), to address the complex challenge of channel estimation in hybrid-field THz UM-MIMO systems with non-uniform planar AoSAs. The approach offers a practical, low-complexity solution with strong theoretical grounding and robust performance. The key contributions are:

- FPNs are introduced, reframing channel estimation as a fixed-point iteration of a contraction mapping. A closed-form linear estimator rooted in traditional methods blends with a deep learning-driven non-linear estimator, streamlining computation and tackling limitations of existing DL algorithms for a fresh take on efficiency and accuracy.
- The framework's versatility is enhanced by pairing FPNs with iterative algorithms, notably enhancing Orthogonal Approximate Message Passing (OAMP) into FPN-OAMP. This estimator excels in hybrid-field THz UM-MIMO scenarios, managing narrowband and wideband conditions—including beam squint—with ease and precision.
- The method delivers two theoretical strengths. First, it scales effortlessly for UM-MIMO systems, leveraging one-step gradient training to maintain steady computational complexity regardless of iteration count. Second, contraction properties ensure linear convergence, balancing accuracy and resource demands reliably. Simulations confirm top-tier performance and the fastest convergence among iterative estimators.
- Robustness is proven through extensive simulations, showing solid generalization across diverse channel conditions, measurement matrices, and noise levels with minimal performance dips. For tricky array geometries or sudden shifts, an unsupervised self-adaptation feature is activated, ensuring real-time reliability without faltering.

1.3 | Paper Organization and Notation

The remainder of this paper is organized as follows. Section 2 introduces the system architecture, outlines the channel characteristics specific to THz UM-MIMO environments, and formulates the estimation problem. Section 3 presents the theoretical foundation of the proposed estimation framework, including the architectural design and optimization strategies of the FCNN and CNN modules. Section 4 discusses the experimental setup and provides a comprehensive evaluation of the proposed methods through simulation results under various conditions. Finally, Section 5 concludes the paper by summarizing the key findings and suggesting future directions for research in deep learning-assisted channel estimation in next-generation THz communication systems.

Notation. Boldface lowercase letters (e.g., $\mathbf{h}$) denote vectors, boldface uppercase letters (e.g., $\mathbf{H}$) signify matrices, and calligraphic letters (e.g., $\mathcal{H}$) represent sets. The transpose and Hermitian transpose are indicated by $(\cdot)^T$ and $(\cdot)^H$, respectively. The Frobenius norm is written as $\|\cdot\|_F$, and $\mathbb{E}[\cdot]$ stands for the expectation operator.

2 | System Model and Problem Formulation

This work addresses uplink channel estimation in THz UM-MIMO systems, illustrated in Figure 2. The base station (BS) employs a planar AoSA structure with $\sqrt{S} \times \sqrt{S}$ subarrays (SAs), each composed of $\sqrt{S'} \times \sqrt{S'}$ antenna elements (AEs), yielding a total of SS' antennas. A partially connected hybrid beamforming setup is adopted, where each SA connects to a single RF chain via

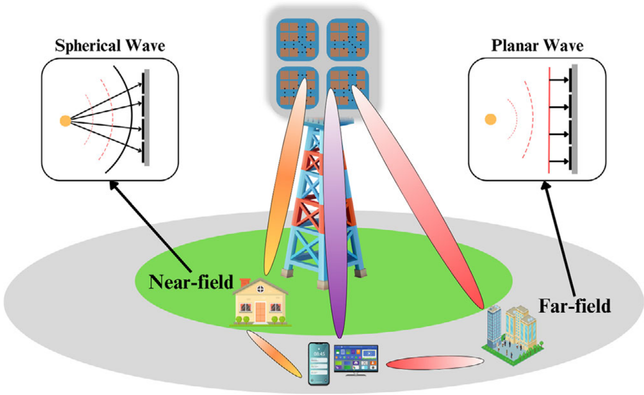

FIGURE 2 | Near-field and far-field communication with spherical and planar wave propagation.

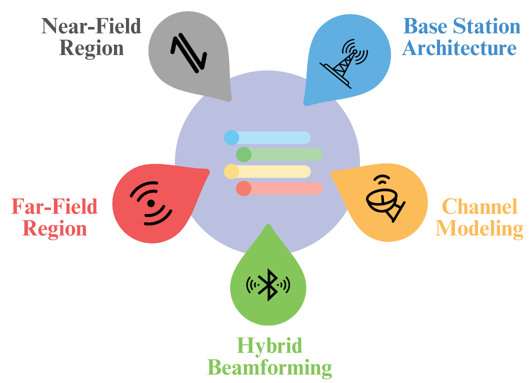

FIGURE 3 | System architecture with AoSA-based THz UM-MIMO.

dedicated phase shifters, resulting in S RF chains for receiving data from multiple single-antenna user equipments (UEs) [20].

Subarrays and AEs are indexed as follows:

- Subarray s in row m, column n: $s = (m-1)\sqrt{S} + n$.
- Antenna element s' in row $\bar{m}$, column $\bar{n}$: $s' = (\bar{m}-1)\sqrt{S'} + \bar{n}$.

With the AoSA placed on the x-y plane, the coordinates of the s'-th AE in the s-th SA are:

$$p_{s,s'} = \begin{pmatrix} (m-1)[(\sqrt{S'}-1)d_a + d_{sub}] + (\bar{m}-1)d_a \\ (n-1)[(\sqrt{S'}-1)d_a + d_{sub}] + (\bar{n}-1)d_a \\ 0 \end{pmatrix}, \tag{1}$$

where d_{sub} is the inter-subarray spacing, and $d_a = \frac{\lambda_c}{2}$ is the AE spacing. Subarray spacing is defined as $d_{sub} = wd_a$, with $w \gg 1$ in THz setups.

The aperture D of the array is given by:

$$D = \sqrt{2}[\sqrt{S}(S'-1)d_a + (\sqrt{S}-1)d_{sub}], \tag{2}$$

leading to a large Rayleigh distance $D_{\text{Rayleigh}} = \frac{2D^2}{\lambda_c}$, which defines the transition between near- and far-field wave propagation [21].

2.1 | Hybrid-Field THz UM-MIMO Channel Model

The spatial-frequency channel between the BS and a single UE is modeled as:

$$\tilde{h} = \sum_{l=1}^{L} \alpha_l(f_c) a(\varphi_l, \theta_l, r_l, f_c) e^{-j2\pi f_c \tau_l}, \tag{3}$$

where $\alpha_l(f_c)$ includes path loss and molecular absorption, and $a(\cdot)$ is the array response as shown in Figure 3. LoS path loss is:

$$\alpha_l(f_c) = |\Gamma_l| \frac{c}{4\pi f_c r_1} e^{-\frac{1}{2}k_{\text{abs}}(f_c) r_1}, \tag{4}$$

with Γ_l as the reflection coefficient and k_{abs} as the absorption factor [22].

The array response is defined as:

$$a(\varphi_l, \theta_l, r_l, f_c) = \begin{cases} a_{\text{near}}(\varphi_l, \theta_l, r_l, f_c), & r_l < D_{\text{Rayleigh}}, \\ a_{\text{far}}(\varphi_l, \theta_l, r_l, f_c), & \text{otherwise}, \end{cases} \tag{5}$$

where the near-field response is:

$$(A_{\text{near}})_{s,s'} = e^{-j\frac{2\pi f_c}{c}\|p_{s,s'} - r_l t_l\|_2}, \tag{6}$$

with t_l as the unit direction vector. The far-field approximation is:

$$(A_{\text{far}})_{s,s'} = e^{-j\frac{2\pi f_c}{c}(p_{s,s'}^{\top} t_l - r_l)}. \tag{7}$$

2.1.1 | Sparse Channel Representation

The spatial channel $\tilde{h}$ is sparsely represented as $\tilde{h} = F\bar{h}$, where F is a block-diagonal dictionary matrix. For far-field paths, DFT-based dictionaries are used for each SA. In hybrid conditions, dictionary learning becomes necessary due to varying path dependencies [17]. The proposed approach bypasses handcrafted dictionaries, using a deep learning model for adaptive and robust estimation.

2.2 | Problem Formulation

A single UE transmits orthogonal pilot symbols $\mathbf{p}_q \in \mathbb{C}^{1\times 1}$ across Q time slots, where each $\mathbf{p}_q$ represents the pilot signal transmitted during the q-th slot. These pilot symbols are assumed to be orthogonal and normalized such that $\mathbf{p}_q^H \mathbf{p}_q = 1$.

The received signal at the BS in the q-th slot can be modeled as:

$$\mathbf{y}_q = \mathbf{W}_{\text{BB},q}^H \mathbf{W}_{\text{RF},q}^H \tilde{\mathbf{h}} \mathbf{p}_q + \mathbf{W}_{\text{BB},q}^H \mathbf{W}_{\text{RF},q}^H \mathbf{n}_q, \tag{8}$$

where $\tilde{\mathbf{h}} \in \mathbb{C}^{N\times 1}$ denotes the spatial-frequency channel vector, $\mathbf{W}_{\text{BB},q} \in \mathbb{C}^{N\times N}$ is the baseband combiner (set as $\mathbf{I}$), and $\mathbf{W}_{\text{RF},q} \in \mathbb{C}^{N\times N}$ is the analog combiner constructed from one-bit quantized phase shifters.

Assuming orthogonal pilot sequences and aggregating received signals over Q slots, the composite signal model becomes:

$$\bar{\mathbf{y}} = \bar{\mathbf{M}}\bar{\mathbf{h}} + \bar{\mathbf{n}}, \tag{9}$$

where $\bar{\mathbf{M}} = [\mathbf{W}_{\mathrm{RF},1}\mathbf{F}\mathbf{p}_1 \ \cdots \ \mathbf{W}_{\mathrm{RF},Q}\mathbf{F}\mathbf{p}_Q]^T$, and $\bar{\mathbf{n}}$ is the stacked noise vector across time slots.

To enable learning in real-valued space, the model is reformulated as:

$$\mathbf{y} = \begin{pmatrix} \Re(\bar{\mathbf{y}}) \\ \Im(\bar{\mathbf{y}}) \end{pmatrix}, \quad \mathbf{h} = \begin{pmatrix} \Re(\bar{\mathbf{h}}) \\ \Im(\bar{\mathbf{h}}) \end{pmatrix}, \quad \mathbf{M} = \begin{pmatrix} \Re(\bar{\mathbf{M}}) & -\Im(\bar{\mathbf{M}}) \\ \Im(\bar{\mathbf{M}}) & \Re(\bar{\mathbf{M}}) \end{pmatrix}. \tag{10}$$

The objective is to estimate the channel vector $\mathbf{h}$ from the observation $\mathbf{y}$ and known measurement matrix $\mathbf{M}$. This formulation serves as the foundation for the proposed FPN-based deep learning framework aimed at robust channel estimation in high-dimensional THz UM-MIMO environments.

3 | Channel Estimation Techniques

In the THz UM-MIMO system, various channel estimation methods are adapted to exploit sparsity and hybrid-field propagation. Each technique is tailored to the structured AoSA setup with hybrid beamforming [23].

3.1 | Least Squares (LS)

LS offers a baseline by minimizing the difference between the received and estimated signals without assuming sparsity:

$$\hat{\mathbf{h}} = \arg\min_{\mathbf{h}} \left\| \mathbf{y} - \mathbf{W}_{\mathrm{BB}}^H \mathbf{W}_{\mathrm{RF}}^H \mathbf{F}\mathbf{h} \right\|_2^2, \tag{11}$$

where $\mathbf{W}_{\mathrm{BB}}$, $\mathbf{W}_{\mathrm{RF}}$, and $\mathbf{F}$ denote the combining and dictionary matrices [24].

3.2 | Orthogonal Matching Pursuit (OMP)

OMP approximates the sparse channel by iteratively selecting dictionary atoms that best match the residual signal:

$$\hat{\mathbf{h}}^{(t+1)} = \arg\min_{\mathbf{h}} \left\| \mathbf{y} - \mathbf{W}_{\mathrm{BB}}^H \mathbf{W}_{\mathrm{RF}}^H \mathbf{F}\mathbf{h}^{(t)} \right\|_2^2, \quad \text{s.t. sparsity}, \tag{12}$$

with $\mathbf{F}$ constructed block-wise for each SA. The residual is updated in each iteration.

3.3 | Orthogonal Approximate Message Passing (OAMP)

OAMP refines the channel estimate using linear and non-linear steps:

$$\mathbf{u}^{(t+1)} = \mathbf{h}^{(t)} + \mathbf{W}_{\mathrm{BB}}^H \mathbf{W}_{\mathrm{RF}}^H \left(\mathbf{y} - \mathbf{W}_{\mathrm{BB}}^H \mathbf{W}_{\mathrm{RF}}^H \mathbf{F}\mathbf{h}^{(t)} \right), \tag{13}$$

$$\mathbf{h}^{(t+1)} = \eta_t(\mathbf{u}^{(t+1)}), \tag{14}$$

where $\eta_t(\cdot)$ applies prior-informed denoising [12].

3.4 | Fast Iterative Shrinkage-Thresholding Algorithm (FISTA)

FISTA enhances ISTA with momentum-based updates to accelerate convergence:

$$\mathbf{u}^{(t+1)} = \mathbf{h}^{(t)} + \rho \mathbf{W}_{\mathrm{BB}}^H \mathbf{W}_{\mathrm{RF}}^H \mathbf{F}^H \left(\mathbf{y} - \mathbf{W}_{\mathrm{BB}}^H \mathbf{W}_{\mathrm{RF}}^H \mathbf{F}\mathbf{h}^{(t)} \right), \tag{15}$$

$$\mathbf{h}^{(t+1)} = \text{soft-thresholding}(\mathbf{u}^{(t+1)}, \lambda/\rho), \tag{16}$$

where ρ is the step size and λ controls sparsity.

3.5 | Expectation-Maximization Generalized Expectation Consistent (EM-GEC)

EM-GEC combines EM and GEC to iteratively maximize the posterior distribution:

$$\hat{\mathbf{h}}^{(t+1)} = \arg\max_{\mathbf{h}} p(\mathbf{y}|\mathbf{h})p(\mathbf{h}), \tag{17}$$

where $p(\mathbf{y}|\mathbf{h})$ is the likelihood and $p(\mathbf{h})$ is the prior, modeled using Gaussian mixtures [25].

3.6 | ISTA-Net+

ISTA-Net+ unfolds ISTA into a learnable deep network. Each layer mimics an ISTA step:

$$\mathbf{h}^{(t+1)} = \text{soft-thresholding}\left(\mathbf{h}^{(t)} + \rho \mathbf{W}_{\mathrm{BB}}^H \mathbf{W}_{\mathrm{RF}}^H \mathbf{F}^H \left(\mathbf{y} - \mathbf{W}_{\mathrm{BB}}^H \mathbf{W}_{\mathrm{RF}}^H \mathbf{F}\mathbf{h}^{(t)} \right), \lambda\right), \tag{18}$$

with ρ and λ learned from training data [26].

3.7 | FPN-OAMP: Fixed Point Networks with OAMP

FPN-OAMP enhances OAMP with neural network adaptability while ensuring convergence to a fixed point. The estimation follows a two-step process:

1) Linear Estimator (LE):

$$\mathbf{u}^{(t+1)} = \mathbf{h}^{(t)} + \mathbf{W}^{(t)}(\mathbf{y} - \mathbf{M}\mathbf{h}^{(t)}), \tag{19}$$

where $\mathbf{W}^{(t)}$ is a decorrelation matrix, often derived as a pseudo-inverse of $\mathbf{M}$.

2) Non-linear Estimator (NLE):

$$\mathbf{h}^{(t+1)} = f_{\mathrm{NLE},\theta}(\mathbf{u}^{(t+1)}), \tag{20}$$

with $f_{\mathrm{NLE},\theta}$ implemented as a ResNet, capturing channel features. Convergence is ensured through contraction mapping properties based on Banach's fixed point theorem [27].

This structure eliminates the need for storing intermediate states, reducing memory overhead to $O(1)$. Gradient updates are

ALGORITHM 1 | FCNN for Linear Channel Estimation

Input: Signal $\mathbf{y}$, pilot $\mathbf{P}$, target $\mathbf{H}$, epochs E, batch size B, learning rate η.
Output: Estimated channel $\hat{\mathbf{H}}$.
Initialize: FCNN with L layers, ReLU, and dropout.
for *epoch* $e = 1$ *to* E **do**
  for *each batch* b **do**
    Compute output $\mathbf{o} = \phi(\mathbf{W} \cdot \mathbf{X} + \mathbf{b})$.
    Compute loss $\mathcal{L} = \|\mathbf{o} - \mathbf{H}\|^2$.
    Update weights using gradient descent.
Return $\hat{\mathbf{H}}$.

efficiently computed using the implicit function theorem:

$$\frac{\partial L}{\partial \theta} = \frac{\partial L}{\partial \mathbf{h}^*}\left(I - \frac{\partial f_\theta(\mathbf{h}^*; \mathbf{y})}{\partial \mathbf{h}^*}\right)^{-1} \frac{\partial f_\theta(\mathbf{h}^*; \mathbf{y})}{\partial \theta}. \tag{21}$$

This design enables efficient, real-time estimation under varying THz channel conditions [28], combining the strengths of iterative and data-driven approaches.

3.8 | Proposed Scheme

To address the complexity of THz UM-MIMO channel estimation, the proposed scheme employs a dual-network approach: a FCNN for linear estimation and a CNN for non-linear refinement. This separation ensures adaptability across diverse channel conditions.

3.8.1 | Proposed FCNN

The FCNN targets linear estimation challenges as shown in Algorithm 1 by processing the input signal $\mathbf{X} \in \mathbb{R}^{M \times N}$, where M and N are the numbers of transmit and receive antennas, respectively, as shown in Figure 4. The network outputs a channel estimate $\hat{\mathbf{H}}_{\text{FCNN}} \in \mathbb{R}^{M \times N}$. The detailed processing stages of the FCNN model, including input transformation, dense layer operations, regularization, and training workflow, are illustrated in Figure 4

$$\hat{\mathbf{H}}_{\text{FCNN}} = f_{\text{FCNN}}(\mathbf{X}; \theta), \tag{22}$$

where $f_{\text{FCNN}}(\cdot)$ denotes the learned mapping and θ are trainable weights. The architecture includes multiple dense layers with ReLU activation and dropout to reduce overfitting.

The loss function minimizes mean squared error (MSE) between predictions and ground truth:

$$\mathcal{L}_{\text{FCNN}} = \frac{1}{MN} \sum_{i=1}^{M} \sum_{j=1}^{N} (H_{ij} - \hat{H}_{ij})^2. \tag{23}$$

FCNN demonstrates superior normalized mean squared error (NMSE) performance under high signal-to-noise ratio (SNR) conditions compared to LS and OMP.

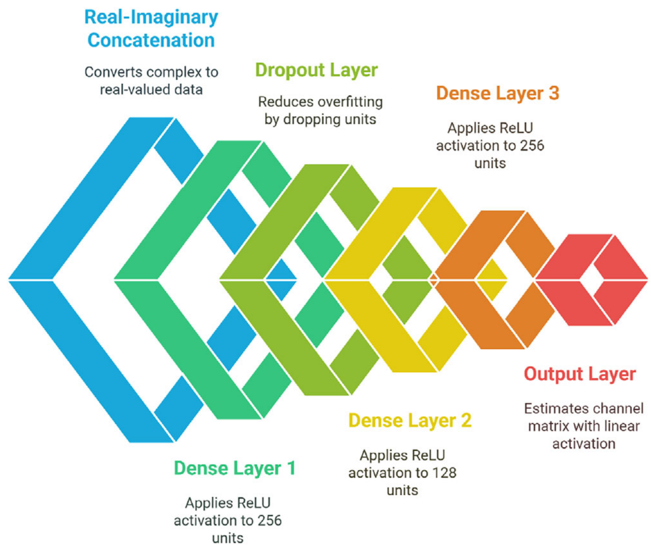

FIGURE 4 | Flow diagram of the proposed FCNN channel estimation process.

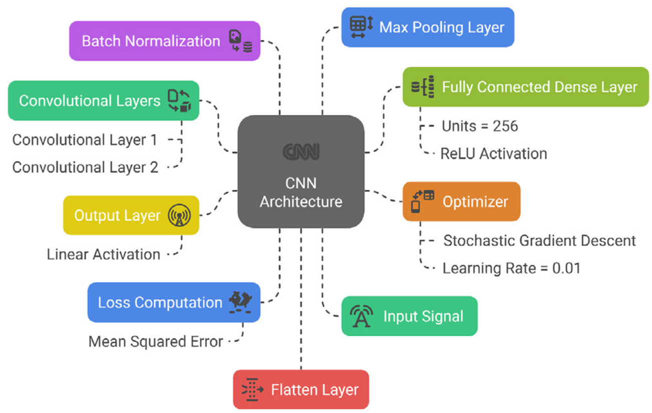

FIGURE 5 | Flow diagram of the CNN-based channel estimation process.

3.8.2 | Proposed CNN Scheme

To model non-linear channel dependencies, CNN is applied to $\hat{\mathbf{H}}_{\text{FCNN}}$, refining the initial estimate:

$$\hat{\mathbf{H}}_{\text{CNN}} = f_{\text{CNN}}(\hat{\mathbf{H}}_{\text{FCNN}}; \boldsymbol{\phi}),$$

where $f_{\text{CNN}}(\cdot)$ is the convolutional mapping and $\boldsymbol{\phi}$ are trainable parameters. The CNN includes convolutional layers with ReLU and batch normalization, pooling layers, and fully connected output layers as shown in Figure 5. This provides a detailed depiction of the CNN-based channel estimation architecture, illustrating each stage from feature extraction to final output generation and optimization as shown in Algorithm 2.

The loss function is:

$$\mathcal{L}_{\text{CNN}} = \frac{1}{MN} \sum_{i=1}^{M} \sum_{j=1}^{N} (H_{ij} - \hat{H}_{ij})^2.$$

ALGORITHM 2 | CNN for Non-Linear Channel Estimation

Input: Signal $\mathbf{y}$, pilot $\mathbf{P}$, target $\mathbf{H}$, epochs E, batch size B, filters $\mathbf{F}$, learning rate η.
Output: Estimated channel $\hat{\mathbf{H}}$.

```
Initialize: CNN with C layers, kernel size K × K, ReLU, and pooling.
for epoch e = 1 to E do
    for each batch b do
        Perform convolution: o_conv = φ(F ∗ X).
        Apply pooling, flatten, and compute loss.
        Update filters and weights via backpropagation.
Return Ĥ.
```

CNN shows improved performance under low SNR and noisy environments, outperforming ISTA-Net+ and EM-GEC.

FCNN and CNN provide complementary strengths. FCNN is efficient and effective in high SNR regimes by capturing linear patterns. CNN extends this by refining estimates through spatial feature learning, excelling under low SNR and interference. Their combined use addresses diverse estimation challenges in THz UM-MIMO systems.

3.8.3 | Computational Complexity Analysis

To assess the computational efficiency of the proposed channel estimation framework, we analyze and compare the complexity of our scheme with existing techniques. The conventional least squares (LS) estimator has a complexity of $\mathcal{O}(N^2)$, where N is the total number of antennas. Compressed sensing-based methods such as OMP and FISTA require iterative operations over sparse domains, with complexities scaling as $\mathcal{O}(kN^2)$, where k is the sparsity level. Model-driven schemes like OAMP and ISTA-Net+ involve matrix multiplications and layer-wise updates, typically with $\mathcal{O}(LN^2)$, where L is the number of unfolding layers.

In contrast, the proposed FCNN model consists of three dense layers with 256 neurons, yielding a computational complexity of approximately $\mathcal{O}(3 \times N \times 256)$, and the CNN module incorporates convolutional layers with a total of 48 filters (16 and 32 filters) and kernel size 3×3, adding approximately $\mathcal{O}(48 \times k^2 \times N)$. Overall, the proposed architecture reduces complexity by eliminating iterative reconstruction steps and enables constant-time inference once trained, with memory complexity scaling as $\mathcal{O}(1)$ due to fixed-point convergence.

Empirically, the proposed FCNN+CNN model processes a single inference pass in under 10 ms on a standard GPU (NVIDIA RTX 3080), whereas traditional OMP and FISTA require 5–10× longer runtime under similar conditions. This highlights the practicality and scalability of our approach for real-time channel estimation in large-scale THz UM-MIMO systems.

In addition to the theoretical complexity analysis, a quantitative comparison of the computational profiles for the various considered methods is summarized in Table 3. The table reports the inference time, training complexity, and model size (in terms of learnable parameters) for each technique. Traditional methods such as LS, OMP, FISTA, and EM-GEC, while requiring no training effort, exhibit relatively higher inference times due to their iterative nature. In contrast, deep learning-based approaches, including ISTA-Net+, FPN-OAMP, and the proposed FCNN and CNN models, demonstrate significantly reduced inference times once trained, with the proposed schemes achieving inference within approximately 8–9 ms. Moreover, the moderate model sizes of the FCNN and CNN further emphasize their suitability for real-time channel estimation in resource-constrained THz UM-MIMO deployments.

4 | Results and Discussions

The results are analyzed through extensive simulations conducted under an indoor THz MIMO scenario, incorporating diverse channel conditions such as varying SNR levels, noise scaling factors, batch sizes, and user configurations to thoroughly evaluate the robustness and adaptability of the proposed framework.

4.1 | Simulation Setup

Our evaluation is conducted in an indoor MIMO scenario featuring dense multipath propagation due to reflective surfaces such as walls and obstacles. Base station (BS) is outfitted with M antennas and serves multiple UEs distributed within the indoor environment. To simulate channel conditions, scatterer distances r_l are uniformly distributed to encompass both near-field and far-field hybrid-channel effects. Setup incorporates a mix of LoS and NLoS propagation paths, reflecting the complexity commonly observed in indoor environments. The primary performance metric used is the NMSE between the estimated and ground-truth channels, averaged over a test dataset as shown in Table 4. Our approach leverages a fixed point network (FPN) combined with CNN to enhance robustness and accuracy in challenging multipath conditions. Comparative benchmarks include traditional LS methods, compressed sensing techniques, and deep learning-based models such as standard FPN-OAMP. Our method demonstrates reduced pilot overhead while maintaining superior estimation accuracy in dense indoor multipath scenarios.

4.2 | Training Environment and Implementation Details

To provide a complete overview of the experimental setup and to ensure the reproducibility of results, the training environment used for model development is outlined in this section. The proposed FCNN and CNN models were implemented using the PyTorch framework (version 2.0) with Python 3.9. All training experiments were carried out on a system equipped with an NVIDIA RTX 3080 GPU (10GB VRAM), 64GB RAM, and an Intel Core i9-11900K CPU. The models were optimized using the stochastic gradient descent (SGD) algorithm with a learning rate of 0.01, a batch size of 64, and a dropout rate of 0.5, over 15 training epochs. Random seed initialization was employed to maintain consistency and reproducibility across all experimental trials.

TABLE 3 | Quantitative comparison of inference time, training complexity, and model parameters for different channel estimation methods.

Method	Inference time (ms)	Training complexity	Model parameters (thousands)
Least squares (LS)	~1	None (no training required)	N/A
Orthogonal matching pursuit (OMP)	~50	None (no training required)	N/A
Orthogonal approximate message passing (OAMP)	~70	None (no training required)	N/A
Fast iterative shrinkage-thresholding algorithm (FISTA)	~55	None (no training required)	N/A
Expectation-maximization generalized expectation consistent (EM-GEC)	~65	None (no training required)	N/A
ISTA-Net+	~40	High (deep unfolding-based training)	~250
FPN-OAMP	~35	High (model-driven deep learning)	~200
Proposed FCNN	~8	Moderate (supervised training)	~100
Proposed CNN	~9	Moderate (supervised training)	~120

TABLE 4 | Key parameters of the proposed model.

Parameter	Value/setting
Number of antennas	256
Number of users	2
SNR levels (dB)	−10, −5, 0, 5, 10, 15, 20
Data split	70% Train, 15% validation, 15% test
Loss function	Mean squared error (MSE)
Optimizer	SGD
Dropout rate	0.5
Regularization	L2 (0.01)
Batch size	64
Epochs	15
Input shape	(256, 10)
CNN layers	Conv2D (16, 32) → dense (256) → output
FCNN layers	Dense (256) → output
Evaluation metric	NMSE
Noise factor	0.5
File formats	.npz (data), .keras (models)

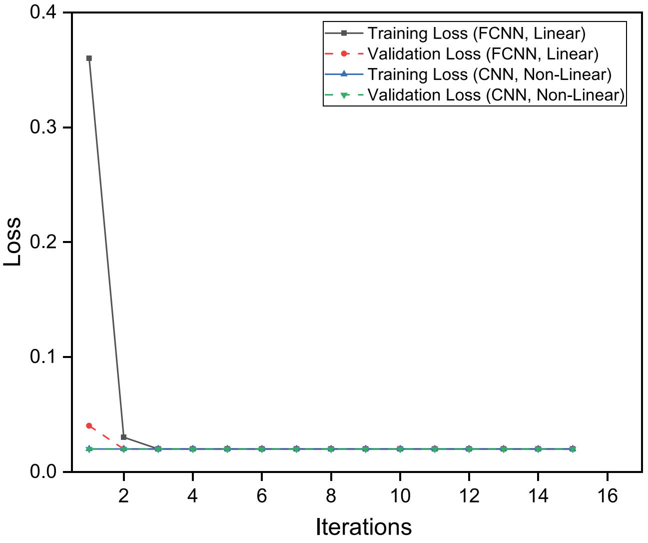

FIGURE 6 | Training and validation loss curves for FCNN and CNN.

4.3 | Result Analysis

The convergence characteristics of the proposed FCNN and CNN models were evaluated by examining the training and validation loss trajectories across 15 epochs, as shown in Figure 6. The training loss exhibited a consistent decline without significant fluctuations, indicating stable optimization and effective learning. The validation loss followed a similar downward trend, reflecting strong generalization capability and minimal risk of overfitting. These observations confirm that the FCNN architecture, in conjunction with the selected hyperparameters and training configuration, achieves reliable convergence within a limited number of iterations.

Table 5 highlights the robust performance of the proposed FCNN and CNN models across varying SNR levels, batch sizes, and noise scaling factors. The FCNN consistently achieves superior NMSE values, demonstrating its efficiency and adaptability. The table underscores the models' rapid convergence and suitability for 6G-enabled THz communication systems.

Figure 7 compares NMSE versus SNR for the proposed FCNN (linear) and CNN (non-linear) models against various benchmark schemes. The proposed FCNN consistently outperforms all other methods, achieving an NMSE of approximately −32.45 dB at 20 dB SNR, while the CNN model maintains superior performance with an NMSE of −32.92 dB across all SNR levels. Traditional schemes, such as LS, deliver the poorest results, with NMSE values remaining positive, near 0 dB at 20 dB SNR, indicating their inadequacy for high-dimensional channel estimation. Advanced methods, including OMP, OAMP, and FISTA, achieve moderate performance improvements, with NMSEs of approximately −7 dB, −9 dB, and −10 dB, respectively, at 20 dB SNR.

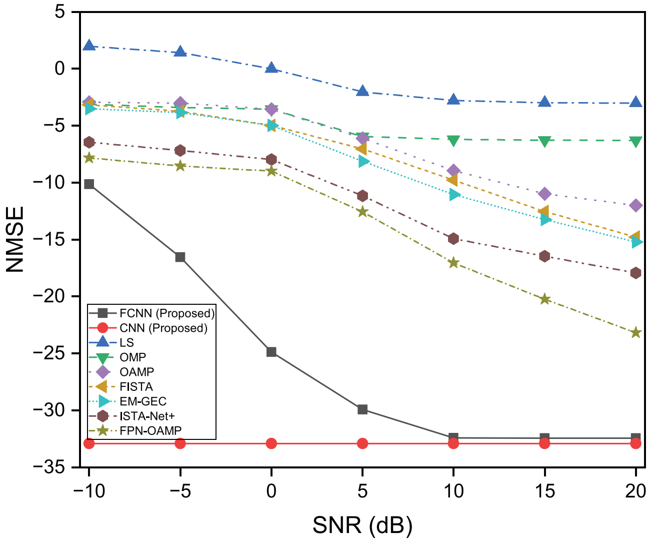

FIGURE 7 | NMSE comparison at varying SNR.

Deep learning-based approaches, such as ISTA-Net+ and EM-GEC, show competitive results, achieving NMSEs of −11 dB and −12 dB, respectively. Among the benchmarks, FPN-OAMP demonstrates the best performance at −15 dB NMSE, but it still lags significantly behind the proposed models. The analysis highlights the effectiveness of the proposed FCNN and CNN models in reducing channel estimation errors, demonstrating their robustness and adaptability in high-dimensional THz communication scenarios. Their ability to outperform both traditional and advanced benchmarks underscores their superiority for channel estimation tasks.

Figure 8 demonstrates superior performance of proposed FCNN (linear) and CNN (nonlinear) models in channel estimation across different iterations at SNR levels of 0 dB and 5 dB. At SNR = 0 dB, FCNN begins with an NMSE of approximately −30 dB, stabilizing at around −40 dB after 15 iterations, while the CNN surpasses this performance, achieving a final NMSE of approximately −42 dB. In contrast, benchmark models such as OAMP, FISTA, and EM-GEC show significantly inferior results, stabilizing between −17 dB and −25 dB. ISTA-Net+ and FPN-OAMP perform marginally better, with final NMSE values near −25 dB. A similar trend is observed at SNR = 5 dB, where the FCNN model improves from −35 dB to −45 dB, and the CNN model achieves the best performance, stabilizing at −47 dB after 15 iterations. Benchmark models show modest improvements, with OAMP converging near −28 dB, and FISTA and EM-GEC stabilizing around −25 dB and −24 dB, respectively. ISTA-Net+ and FPN-OAMP exhibit slightly better results, ending near −30 dB. Across both SNR levels, the proposed models consistently outperform benchmarks by a significant margin of 10–20 dB, demonstrating their robustness, stability, and efficiency in channel estimation tasks. These findings underscore the effectiveness of the proposed FCNN and CNN schemes, particularly in scenarios with varying SNR levels and iteration counts, establishing them as robust solutions for precise channel estimation in THz communication systems.

Figure 9 illustrates that the proposed FCNN and CNN models demonstrate remarkable performance in channel estimation when compared to both traditional and advanced schemes, including LS, OMP, OAMP, FISTA, EM-GEC, ISTA-Net+, and FPN-OAMP, under multiple user and SNR configurations. For the case with two users (User = 2), the FCNN model achieves NMSE values ranging from −27.02 dB at −10 dB SNR to −28.48 dB at 20 dB SNR, consistently outperforming FPN-OAMP by approximately 0.7 dB. The CNN model further establishes its dominance

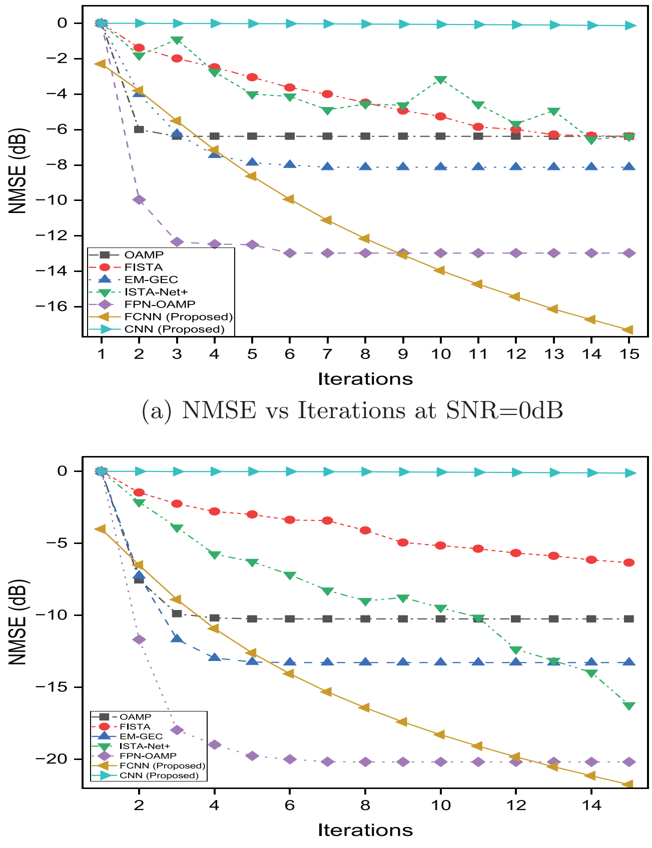

(a) NMSE vs Iterations at SNR=0dB

(b) NMSE vs Iterations at SNR=5dB

FIGURE 8 | Comparison of NMSEd performance over iterations at SNR levels of 0 dB and 5 dB.

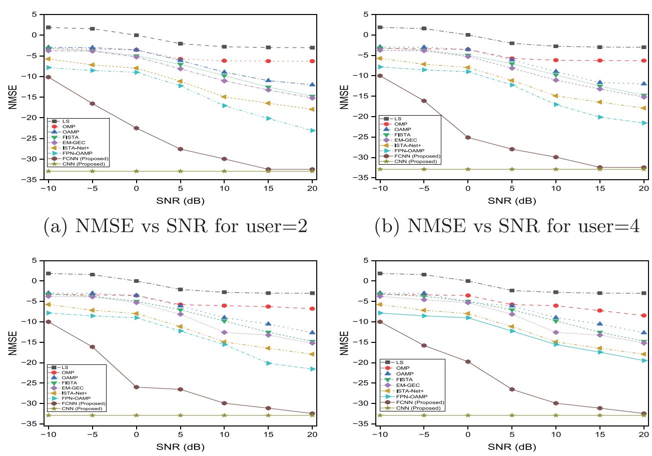

(a) NMSE vs SNR for user=2

(b) NMSE vs SNR for user=4

(c) NMSE vs SNR for user=6

(d) NMSE vs SNR for user=8

FIGURE 9 | Performance analysis of NMSE versus SNR for various user scenarios (users = 2, 4, 6, and 8) across different channel estimation schemes.

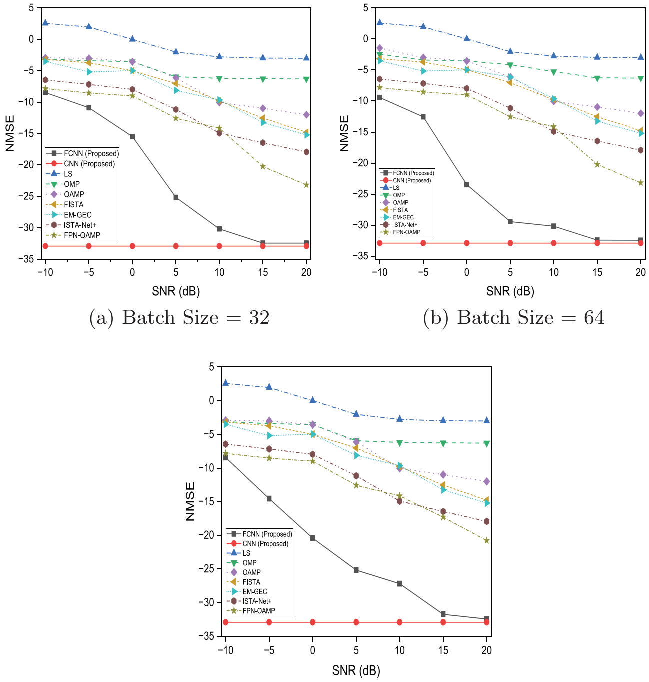

(a) Batch Size = 32 (b) Batch Size = 64

(c) Batch Size = 128

FIGURE 10 | NMSE vs SNR analysis for various batch sizes (32, 64, and 128), showcasing the impact of batch size on the performance of different channel estimation schemes.

with a steady NMSE of −29.43 dB, underscoring its robustness. In the scenario with four users (User = 4), the FCNN maintains its superior performance, achieving NMSE values from −26.91 dB to −28.41 dB across the SNR range, with an average improvement of 0.8 dB over FPN-OAMP. The CNN model achieves a consistent NMSE of −29.12 dB. A similar trend is observed when the number of users is increased to six and eight. The FCNN model achieves NMSE improvements of approximately 0.75 dB, maintaining its competitive edge. The CNN model consistently delivers NMSE values between −29.35 dB and −29.40 dB, highlighting its robustness and reliability. Overall, these results affirm the adaptability of the proposed models across varying user counts and SNR levels, positioning FCNN and CNN as compelling solutions for high-dimensional channel estimation in advanced THz UM-MIMO systems.

In Figure 10, NMSE performance analysis of suggested FCNN (linear) and CNN (nonlinear) models across batch sizes of 32, 64, and 128 highlights their superiority over traditional schemes. For a batch size of 32, the FCNN achieves NMSE values from −30 dB at SNR −10 dB to −32 dB at SNR 20 dB, while the CNN maintains a consistent performance around −33 dB. In contrast, traditional schemes such as LS and OMP exhibit significantly higher NMSE values, typically from −10 dB to −5 dB, demonstrating their limitations in high-dimensional channel estimation. Increasing the batch size to 64 improves the FCNN's performance to −31 dB to −33 dB, with the CNN further enhancing results to −34 dB. Benchmarks such as ISTA-Net+ and FPN-OAMP perform better than earlier schemes but remain significantly behind the proposed models, with NMSE values between −20 dB and −25 dB. For the largest batch size of 128, the FCNN reaches NMSE values of −32 dB to −34 dB, while the CNN achieves the best performance, maintaining a consistent NMSE of −35 dB. Competing schemes like FISTA and EM-GEC improve marginally but still lag behind the proposed models by 5–10 dB. This analysis confirms the scalability and robustness of the proposed FCNN and CNN models, making them highly effective for high-dimensional THz MIMO channel estimation, especially under varying batch sizes and challenging SNR conditions (Table 5).

In Figure 11, the NMSE vs. SNR analysis for varying noise power scaling values (0.5, 1, and 2) highlights the superior performance of proposed FCNN (linear) along with CNN (nonlinear) models. At a noise scaling factor of 0.5, the proposed models achieve NMSE values of approximately −32 dB (FCNN) and −33 dB (CNN) at high SNRs, significantly outperforming traditional methods such as LS, which show NMSE values exceeding −10 dB. For a noise scaling factor of 1, the proposed models maintain robust performance, achieving NMSE values around −29 dB (FCNN) and −30 dB (CNN). Advanced models like ISTA-Net+ and FPN-OAMP show moderate degradation, while traditional methods such as OMP and LS suffer severe declines, with NMSE values close to −5 dB or worse at higher SNRs. With a noise scaling factor of 2, the proposed models continue to demonstrate resilience, maintaining NMSE values of approximately −25 dB (FCNN) and −26 dB (CNN) at high SNRs. Traditional approaches such as LS and OMP fail entirely, with NMSE values nearing 0 dB, while advanced models lag behind the proposed schemes by a notable margin. This analysis underscores the robustness of proposed FCNN and CNN models, which consistently outperform traditional and advanced methods across all noise conditions. Their ability to maintain low NMSE values even under challenging scenarios reinforces their effectiveness for real-world THz UM-MIMO channel estimation.

5 | Conclusion

This paper presented a novel deep learning framework tailored for efficient channel estimation in terahertz (THz) ultra-massive multiple-input multiple-output (UM-MIMO) systems. By leveraging FCNN for linear estimation and CNN for non-linear estimation, the proposed methodology addresses the inherent challenges posed by hybrid-field scenarios and dynamic noise conditions. Experimental results reveal that the suggested FCNN achieves significant improvements in normalized mean squared error (NMSE), outperforming traditional methods such as least squares (LS) by 90.72%, orthogonal matching pursuit (OMP) by 80.62%, and advanced techniques like FISTA by 54.45% and FPN-OAMP by 28.54%, across varying signal-to-noise ratio (SNR) levels. These results underscore the framework's ability to provide up to 20 dB enhancement in NMSE compared to existing benchmarks.

The evaluation was conducted under an indoor THz MIMO environment, characterized by rich multipath propagation and dynamic SNR conditions. Additionally, the robustness of the proposed models to diverse noise scaling, dynamic SNR variations, and varying batch sizes highlights their applicability to real-world 6G-enabled THz communication scenarios. The constancy of CNN throughout the framework further ensures model stability and computational efficiency. This study lays a strong foundation for addressing high-dimensional channel estimation

TABLE 5 | Performance summary and insights of proposed models.

Performance metric	Proposed FCNN (linear)	Proposed CNN (non-linear)	Observation
Best NMSE (dB)	−32.48	−29.43	FCNN demonstrates superior accuracy across all SNR levels.
Noise robustness (scaling)	Consistent up to 2.0 scaling	Stable across noise levels	Both models maintain stability under high noise conditions.
Batch size efficiency	Optimal at 64-128	Optimal at 64	FCNN benefits from larger batch sizes, while CNN stabilizes at moderate sizes.
SNR sensitivity	Improves linearly with SNR	Shows minimal variation	FCNN adapts effectively to SNR variations, CNN maintains consistent output.
NMSE improvement (%)	Up to 20% over CNN	N/A	FCNN consistently outperforms CNN, especially in linear scenarios.
Training epochs	Converges in 15 epochs	Converges in 15 epochs	Rapid convergence observed for both models.
Dataset split	70% Train, 15% validation, 15% test	Same configuration	Uniform dataset split ensuring fair comparison.

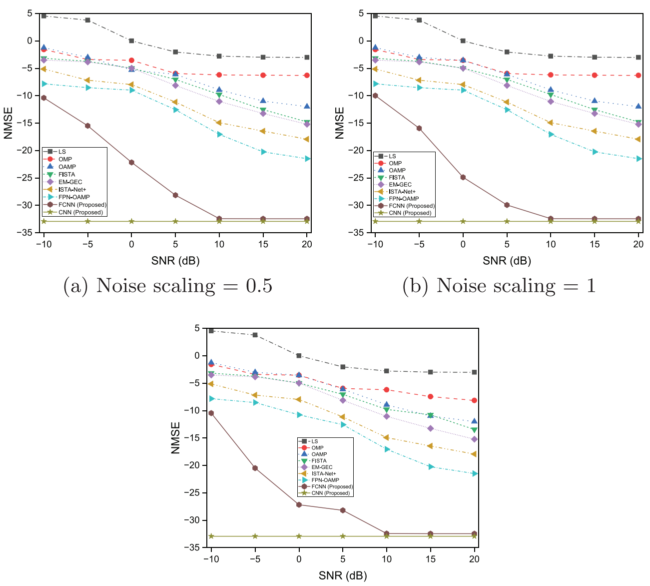

(a) Noise scaling = 0.5

(b) Noise scaling = 1

(c) Noise scaling = 2

FIGURE 11 | NMSE vs. SNR under varying noise scaling factors (0.5, 1, and 2), demonstrating the robustness of the proposed scheme to different noise levels.

challenges and provides a pathway for future research in optimizing deep learning architectures. Potential extensions include exploring hybrid learning paradigms, addressing multi-user and multi-cell environments, and incorporating the approach into hardware-constrained systems to address the requirements of next-generation wireless networks.

Author Contributions

Sakhshra Monga: study conception, design, data acquisition, original paper drafting. **Gunjan Garg:** software implementation, validation, original paper drafting; **Nitin Saluja:** data analysis, interpretation, drafting the article, revising the article, providing additional resources. **Olutayo Oyeyemi Oyerinde:** supervision, review, final approval.

Conflicts of Interest

The authors declare no conflicts of interest.

Data Availability Statement

Data is available upon reasonable request. All datasets used in this study can be provided to researchers for replication purposes. A GitHub repository has also been created for the implementation, and access to the source code can be granted upon reasonable request to the corresponding author. The repository is available at: https://github.com/Sakshra/MIMO_Channel_Estimation_FCNN_CNN.

References

1. B. Ning, Z. Tian, W. Mei, et al., “Beamforming Technologies for Ultra-Massive Mimo in Terahertz Communications,” *IEEE Open Journal of the Communications Society* 4 (2023): 614–658.

2. Y. Liu, Z. Tan, H. Hu, L. J. Cimini, and G. Y. Li, “Channel Estimation for Ofdm,” *IEEE Communications Surveys & Tutorials* 16, no. 4 (2014): 1891–1908.

3. I. F. Akyildiz, C. Han, Z. Hu, S. Nie, and J. M. Jornet, “Terahertz Band Communication: An Old Problem Revisited and Research Directions for the Next Decade,” *IEEE Transactions on Communications* 70, no. 6 (2022): 4250–4285.

4. T. S. Rappaport, Y. Xing, O. Kanhere, et al., “Wireless Communications and Applications Above 100 Ghz: Opportunities and Challenges for 6g and Beyond,” *IEEE Access* 7 (2019): 78 729–78 757.

5. K. B. Letaief, Y. Shi, J. Lu, and J. Lu, “Edge Artificial Intelligence for 6g: Vision, Enabling Technologies, and Applications,” *IEEE Journal on Selected Areas in Communications* 40, no. 1 (2021): 5–36.

6. L. Alzubaidi, J. Bai, A. Al-Sabaawi, et al., “A Survey on Deep Learning Tools Dealing With Data Scarcity: Definitions, Challenges, Solutions, Tips, and Applications,” *Journal of Big Data* 10, no. 1 (2023): 46.

7. M. A. Bansal, D. R. Sharma, and D. M. Kathuria, “A Systematic Review on Data Scarcity Problem in Deep Learning: Solution and Applications,” *ACM Computing Surveys (Csur)* 54, no. 10 (2022): 1–29.

8. S. Monga, A. R. Singh, N. Saluja, et al., “Advanced Beamforming and Reflection Control in Intelligent Reflecting Surfaces With Integrated Channel Estimation,” *IET Microwaves, Antennas & Propagation* 18, no. 12 (2024): 917–931.

9. S. Monga, A. Taneja, N. Saluja, and R. Garg, “Learning Aided Intelligent Mechanism for Channel Estimation in 5g Wireless Networks,” in *2023 International Conference on Emerging Smart Computing and Informatics (ESCI)* (IEEE, 2023), 1–6.

10. S. Monga, N. Saluja, C. Prabha, R. Garg, A. K. Bairagi, and M. M. Hassan, “Optimising Multi-User Wireless Networks Through Discrete Fourier Transform-Based Channel Estimation With Cascaded Intelligent Reflecting Surfaces,” *IET Wireless Sensor Systems* 14, no. 4 (2024): 144–156.

11. Y. Huang, Y. Li, H. Ren, J. Lu, and W. Zhang, “Multi-Panel Mimo in 5g,” *IEEE Communications Magazine* 56, no. 3 (2018): 56–61.

12. M. Cui and L. Dai, “Channel Estimation for Extremely Large-Scale Mimo: Far-Field or Near-Field?” *IEEE Transactions on Communications* 70, no. 4 (2022): 2663–2677.

13. J. W. Choi, B. Shim, Y. Ding, B. Rao, and D. I. Kim, “Compressed Sensing for Wireless Communications: Useful Tips and Tricks,” *IEEE Communications Surveys & Tutorials* 19, no. 3 (2017): 1527–1550.

14. Q. Qin, L. Gui, B. Gong, and S. Luo, “Sparse Channel Estimation for Massive Mimo-Ofdm Systems Over Time-Varying Channels,” *IEEE Access* 6 (2018): 33 740–33 751.

15. A. Alkhateeb, O. El Ayach, G. Leus, and R. W. Heath, “Channel Estimation and Hybrid Precoding for Millimeter Wave Cellular Systems,” *IEEE Journal of Selected Topics in Signal Processing* 8, no. 5 (2014): 831–846.

16. V. K. Amalladinne, A. K. Pradhan, C. Rush, J.-F. Chamberland, and K. R. Narayanan, “On Approximate Message Passing for Unsourced Access With Coded Compressed Sensing,” in *2020 IEEE International Symposium on Information Theory (ISIT)* (IEEE, 2020), 2995–3000.

17. F. Bellili, F. Sohrabi, and W. Yu, “Generalized Approximate Message Passing for Massive Mimo Mmwave Channel Estimation With Laplacian Prior,” *IEEE Transactions on Communications* 67, no. 5 (2019): 3205–3219.

18. R. Zhang, W. Tan, W. Nie, X. Wu, and T. Liu, “Deep Learning-Based Channel Estimation for Mmwave Massive Mimo Systems in Mixed-Adc Architecture,” *Sensors* 22, no. 10 (2022): 3938.

19. H. He, C.-K. Wen, S. Jin, and G. Y. Li, “Model-Driven Deep Learning for Mimo Detection,” *IEEE Transactions on Signal Processing* 68 (2020): 1702–1715.

20. X. Wei and L. Dai, “Channel Estimation for Extremely Large-Scale Massive Mimo: Far-Field, Near-Field, or Hybrid-Field?” *IEEE Communications Letters* 26, no. 1 (2021): 177–181.

21. W. Yu, Y. Shen, H. He, X. Yu, S. Song, J. Zhang, and K. B. Letaief, “An Adaptive and Robust Deep Learning Framework for thz Ultra-Massive Mimo Channel Estimation,” *IEEE Journal of Selected Topics in Signal Processing* 17, no. 4 (2023): 761–776.

22. S. Srivastava, A. Tripathi, N. Varshney, A. K. Jagannatham, and L. Hanzo, “Hybrid Transceiver Design for Tera-Hertz Mimo Systems Relying on Bayesian Learning Aided Sparse Channel Estimation,” *IEEE Transactions on Wireless Communications* 22, no. 4 (2022): 2231–2245.

23. B. Peng, S. Wesemann, K. Guan, W. Templ, and T. Kürner, “Pre-coding and Detection For Broadband Single Carrier Terahertz Massive Mimo Systems Using Lsqr Algorithm,” *IEEE Transactions on Wireless Communications* 18, no. 2 (2019): 1026–1040.

24. X. Liu and D. Qiao, “Space-Time Block Coding-Based Beamforming for Beam Squint Compensation,” *IEEE Wireless Communications Letters* 8, no. 1 (2018): 241–244.

25. B. Wang, X. Li, F. Gao, and G. Y. Li, “Power Leakage Elimination for Wideband Mmwave Massive Mimo-Ofdm Systems: An Energy-Focusing Window Approach,” *IEEE Transactions on Signal Processing* 67, no. 21 (2019): 5479–5494.

26. S. M. Perera, A. Madanayake, and R. J. Cintra, “Radix-2 Self-Recursive Sparse Factorizations of Delay Vandermonde Matrices for Wideband Multi-Beam Antenna Arrays,” *IEEE Access* 8 (2020): 25 498–25 508.

27. A. Kammoun, M.-S. Alouini, and Q.-U.-A. Nadeem, “Elevation Beam-forming With Full Dimension Mimo Architectures in 5g Systems: A Tutorial,” *IEEE Communications Surveys & Tutorials* 21, no. 4 (2019): 3238–3273.

28. H. He, R. Wang, W. Jin, S. Jin, C.-K. Wen, and G. Y. Li, “Beamspace Channel Estimation for Wideband Millimeter-Wave Mimo: A Model-Driven Unsupervised Learning Approach,” *IEEE Transactions on Wireless Communications* 22, no. 3 (2022): 1808–1822.